



Article

Comparison of EV Fast Charging Protocols and Impact of Sinusoidal Half-Wave Fast Charging Methods on Lithium-Ion Cells

Sai Bhargava Althurthi, Kaushik Rajashekara * and Tutan Debnath

Department of Electrical and Computer Engineering, University of Houston, Houston, TX 77204, USA; salthurt@cougarnet.uh.edu (S.B.A.); tdebnath@central.uh.edu (T.D.)

* Correspondence: ksraja@uh.edu

Abstract: In electric vehicle fast charging systems, it is important to minimize the effect of fast charging on the grid and it is also important to operate the charging system at high efficiencies. In order to achieve these objectives, in this paper, a sinusoidal half-wave DC current charging protocol and a sinusoidal half-wave pulsed current charging protocol are proposed for the fast charging of Li-ion batteries. A detailed procedure is presented for implementing the following proposed methods: (a) a pre-defined half-sine wave current function and (b) a pulsed half-sine wave current method. Unlike the conventional full-wave sinusoidal ripple current charging protocols, the proposed study does not utilize any sinusoidal full-wave ripple. The performance of these new charging methods on Ni-Co-Al-type Li-cells is studied and compared with the existing constant current and positive pulsed current charging protocols, which have been discussed in the existing literature. In addition, the changes in the electrochemical impedance spectrograph of each cell are examined to study the effects of the applied charging methods on the internal resistance of the Li cell. Finally, the test results are presented for 250 life cycles of charging at 2C (C: charging rate) and the degradation in cell capacities are compared among the four different methods for the Ni-Co-Al-type Li cell.



Citation: Althurthi, S.B.; Rajashekara, K.; Debnath, T. Comparison of EV Fast Charging Protocols and Impact of Sinusoidal Half-Wave Fast Charging Methods on Lithium-Ion Cells. *World Electr. Veh. J.* **2024**, *15*, 54. <https://doi.org/10.3390/wevj15020054>

Academic Editors: Tao Chen, Xiangjun Quan and Yuanshi Zhang

Received: 31 December 2023
Revised: 27 January 2024
Accepted: 1 February 2024
Published: 6 February 2024



Copyright: © 2024 by the authors. Licensee MDPI, Basel, Switzerland. This article is an open access article distributed under the terms and conditions of the Creative Commons Attribution (CC BY) license (<https://creativecommons.org/licenses/by/4.0/>).

Keywords: fast charging protocols; pulsed charging; battery lifetime; sinusoidal half-wave

1. Introduction

Li-ion battery technology is widely used in electric vehicles (EVs) because of the higher energy density and better battery lifetime. Among the Li-ion chemistries, NMC (Ni-Mn-Co) and NCA (Ni-Co-Al) types are well known for their energy densities, while the LFP (Li-Fe-P) type is best known for its higher number of life cycles. For the widespread adoption of electric vehicles, the role of EV fast charging technology is crucial to minimize the charging time for EVs. Accordingly, based on the charging power levels, several types of EV fast chargers are already available in the market [1]. The research on Level-3 ultra-fast off-board charging attracted great interest in recent years because of its projected ability to reduce charging times (<15 min using >350 kW power-rated chargers) for EVs. Attempts are being made to increase the EV penetration in the transportation sector by addressing the range anxiety experienced by customers. However, such ultra-high-power charging significantly affects the battery lifetime, and, hence, the future cost of the battery [2]. Moreover, the unplanned addition of such high-power chargers to the grid will cause more complications in grid management [3]. Therefore, the impact of these two scenarios should be carefully investigated before a massive deployment of ultra-high-power EV chargers.

In order to develop an effective fast charging method, researchers have been experimenting with several kinds of fast charging protocols [4–6]. The main role of any new charging protocol is to minimize the charging rate (C-rate) impact on battery lifetime degradation and to achieve an energy-efficient charging protocol compared to the traditional constant current–constant voltage (CC-CV) charging method. However, recently,

the pulsed-current charging (PCC) protocol became popular among researchers because of its positive impact on extending the battery lifetime for Li cells [7]. The authors in [8–10] presented a Li-ion cell lifetime extension with the PCC protocol tested on NMC-type Li cells. The impact of the variation of pulse frequencies while charging the Li cell on its lifetime is extensively studied in [9,10]. The effects of PCC on the performance parameters, such as charging speed and impedance analysis, of Li-ion batteries are also equally important [11,12], and this performance evaluation also includes the study of electrochemical impedance spectrographs (EISs) for Li-ion cells [13,14]. Particularly in the impedance spectrographs shown in Figure 1, the radius of the semicircle in the medium-frequency range is crucial, as it signifies the variation in the charge transfer resistance of the cell. This charge transfer resistance, in turn, indicates the rate of capacity fade in the Li-ion cell [14]. Additionally, from Figure 1, the ohmic effect can be estimated from the x-intercept of the Nyquist curve, which is also an essential parameter for estimating the power losses incurred during the charging cycle. The authors in [15] discuss the performance metrics of PCC compared with other pulsed charging protocols like sinusoidal ripple current (SRC) and negative-pulsed charging (NPC). In the SRC method, a sinusoidal full-wave ripple is overlapped on a constant DC current, and the impact of such a charging current on the battery performance is studied in [16,17]. However, none of the above-mentioned charging methods have discussed or implemented the sinusoidal half-wave positive-pulse current charging (SPCC) technique, which is investigated in detail in this paper.

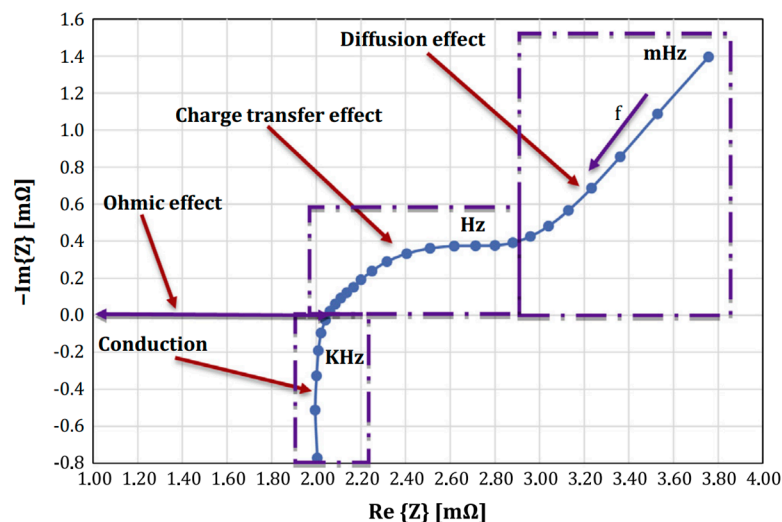


Figure 1. An example of a Nyquist plot from an impedance spectrograph for a Li cell [14].

Apart from the above-discussed pulsed charging protocols, there are algorithm-based charging methods that rely on the state of charge (SoC) of the battery [18,19]. In [19], a universal voltage charging (UVC) protocol is proposed in which the charging current varies as a function of the battery terminal voltage. In the UVC method, the charging current gradually increases at the start and reaches the peak value near to nominal voltage, and slowly falls back to zero as the terminal voltage approaches the maximum set point. Unlike the UVC method, the SCC method proposed in this paper follows a sinusoidal half-wave current function. Relatively, the peak current value of the SCC method is lower than the peak current value of the UVC method. Also, this proposed SCC method is different from the traditional rectangular block-shaped constant current (CC) charging technique.

In the evaluation of any charging method, the CC-CV method is taken as the base case for comparison, since it is the only method that is widely practiced for EV charging. It is well known that in the CC-CV method, the CC phase is the bulk-charging phase that helps in reaching an SoC approximately close to 80% within a short time, whereas the next CV phase takes more time to reach from 80% to 100% SoC or full charging state. Therefore, most of the fast charging protocols in the literature focus on the improvement

of the CC-phase. The focus of this work is to evaluate the performance of new charging methods, and compare the results with the existing CC charging and its equivalent pulsed charging protocols. Hence, the subsequent CV phase is not considered in this work.

To evaluate the impact of the SCC and SPCC protocols on the performance of the Li-ion cells, this paper is organized as follows: Section 2 describes the details of the fast charging protocols implemented and provides a comparison of these protocols. Section 3 presents the detailed experimental steps followed in this evaluation of the fast charging methods, which includes life cycle depth of discharge (DoD) testing along with regular EIS testing of each Li-ion cell. Section 4 provides the experimental results and discussion, and Section 5 concludes the paper.

2. Fast Charging Protocols

A typical CC-mode fast charging phase for a standard Li-ion cell is shown in Figure 2a. In general, for any CC charging phase, a constant charging current of I_{ch} is maintained in the battery cell until the cell reaches its maximum terminal voltage level, V_{max} , as shown in Figure 2a. Therefore, this CC method also uses the V_{max} voltage level as a set point for the charge cycle termination. At the end of each CC charging cycle, the charging time T_{ch} and the amount of charge acquired ΔQ_{ch} is noted by the testing platform, and these parameters are used as the base values for the other three charging methods (SCC, PCC, SPCC). In the other three charging methods, the charging cycle is terminated once the charge acquired by the battery cell is ΔQ_{ch} within the same T_{ch} time (i.e., the charging time measured in the CC method). Thus, an exact comparison is drawn among all four charging methods and is presented in this work.

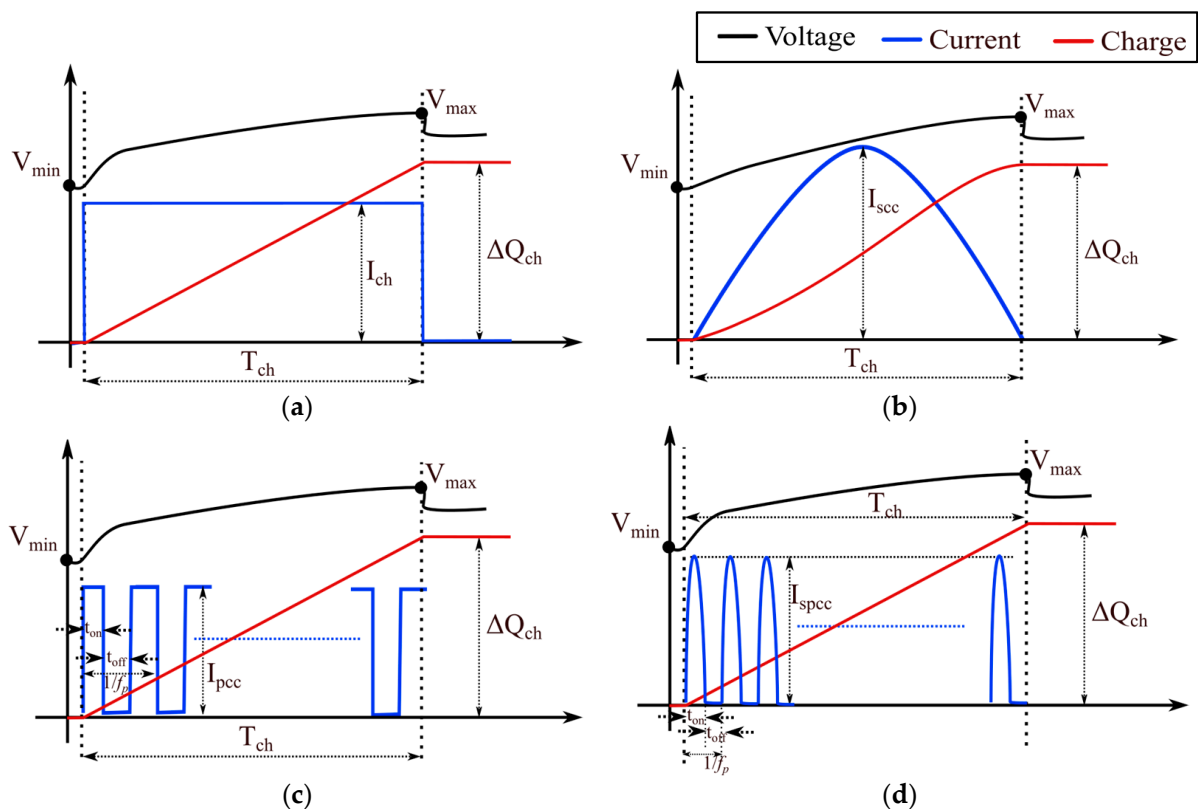


Figure 2. Fast charging protocols evaluated in this work: (a) CC method; (b) SCC method; (c) PCC method; and (d) SPCC method. (Note: T_{ch} is the charge time incurred in the CC method, which is the base value for all of the other three charging methods.)

In the SCC method, the constant charging current is replaced by a sinusoidal half-wave current, as shown in Figure 2b. To acquire the same ΔQ_{ch} within the T_{ch} time, the required peak magnitude of the sine wave I_{SCC} can be calculated from (1), below.

$$\Delta Q_{ch} = I_{ch} \times T_{ch} = \int_0^{T_{ch}} I_{SCC} \times \sin\left(\frac{2\pi t}{T_{ch}}\right) dt \quad (1)$$

$$I_{SCC} = 1.57 \times I_{ch} \quad (2)$$

Similarly, to implement the PCC method for the same ΔQ_{ch} charge within the same T_{ch} time, from a 50% duty cycle positive pulse train, the current pulse magnitude should be twice the value of I_{ch} , as shown in Figure 2c, where f_p is the frequency of the pulse train, and t_{on} and t_{off} are the pulse times ensuring a 50% duty cycle. In the SPCC method, the positive pulses of the PCC method are replaced with equivalent sinusoidal half-wave pulses, as shown in Figure 2d. The effective peak value of the sinusoidal half-wave pulses I_{SPCC} can also be found using a similar relation of Equation (1).

3. Experimental Evaluation

This section explains the detailed step-by-step experimental procedure followed in implementing the above-mentioned charging protocols using a four-module Arbin battery tester setup, as shown in Figure 3. The detailed specifications of the Li-ion cell used in this experiment are listed in Table 1. The algorithms of the charging protocols are programmed on the integrated software of the Arbin battery tester (Figure 3a). The test signals from the tester are then transmitted to the thermal chamber through the output channels of the tester panel. The cable connectors (along with instrumentation) and the four output channels of the Arbin tester panel are shown in Figure 3b. The test signals are received by the four battery-holding modules, which are kept inside the thermal chamber, as shown in Figure 3c. In Figure 3d, a zoomed view of a single Li cell model is presented, illustrating the wiring for the voltage, current, and cell surface temperature sensors.

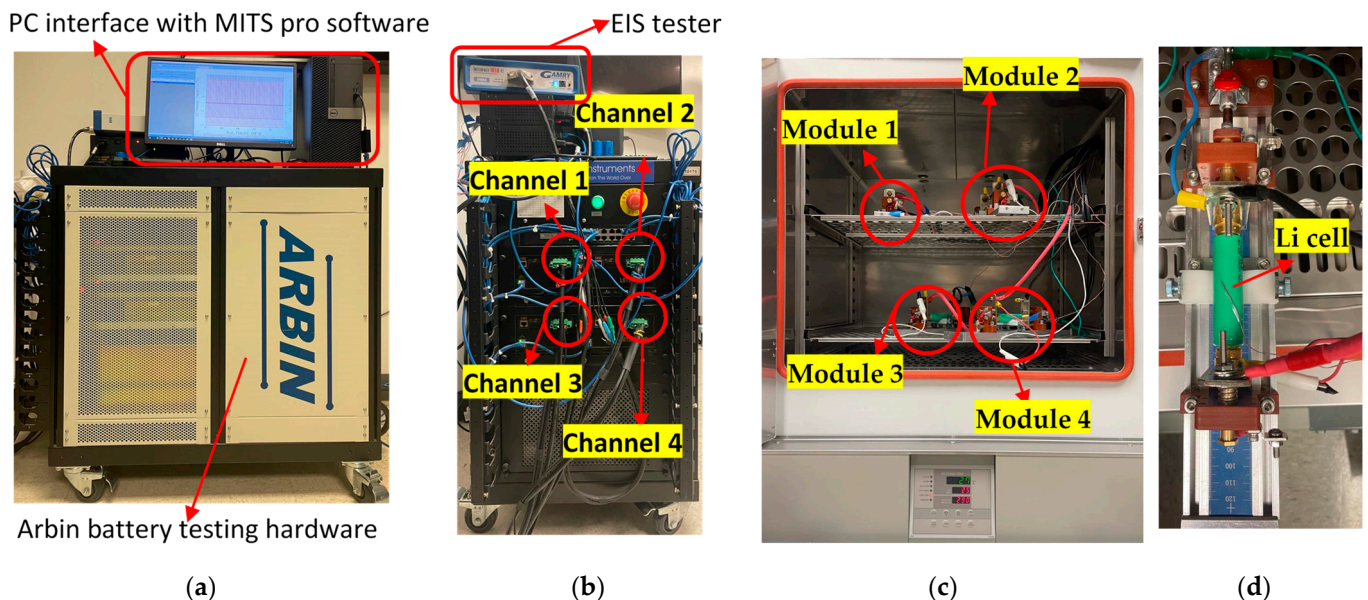


Figure 3. Experimental setup. (a) Arbin battery testing setup; (b) front view of the tester panel; (c) Li cell modules under testing inside the thermal chamber; and (d) single module of a Li cell under testing.

Table 1. Specifications of the Li-ion cell used in the experiment.

Parameter	Value
Model name (Samsung)	INR18650-25R
Electrode chemistry	NCA
Nominal capacity	2.5 Ah
Nominal voltage	3.6 V
Charging cut-off voltage, V_{\max}	4.2 V
Discharging cut-off voltage, V_{\min}	2.5 V
Maximum discharging current	20 A

In this study, the fast charging protocols on the Li-ion cells are tested at a 2C charging rate. Accordingly, the required I_{ch} current for a 2.5 Ah Li-ion cell is 5A in the CC method. Thus, for the PCC method, the corresponding current peak is 10 A when the duty ratio of the pulse train is 50%. Similarly, the corresponding I_{SCC} in the SCC method calculated using (2) is 7.8539 A. Hence, considering a peak current limit close to 10 A in the SPCC method, the required ratio between t_{on} and t_{off} is approximate to 4:1, and the exact corresponding peak value of the sine half-wave pulses (I_{SPCC}) is 9.55 A (<10 A). Although the duty ratios of the PCC and SPCC methods are chosen to be 50 and 80 percent, respectively, the pulse cycle frequencies f_p for both methods are fixed at 0.05 Hz [9]. The corresponding current equations for I_{ch} and experimental current values for each method are also tabulated in Table 2. The implementation of the charge and discharge cycles for the proposed protocol is explained in a later section.

Table 2. Charging current for each method.

CC	SCC	PCC	SPCC
I_{ch}	$1.57 \times I_{\text{ch}}$	$I_{\text{ch}} \times (t_{\text{on}} + t_{\text{off}}) / t_{\text{on}}$	$1.57 \times I_{\text{ch}} \times (t_{\text{on}} + t_{\text{off}}) / t_{\text{on}}$
5 A	7.85 A	10 A ($t_{\text{on}} = t_{\text{off}} = 10$ s)	9.55 A ($t_{\text{on}} = 16$ s and $t_{\text{off}} = 4$ s)

3.1. Experimental Procedure

3.1.1. Cyclic Charge and Discharge Testing

All four charging protocols are experimented with at a 2C charging rate (equivalent to 5A current base of the CC method) and discharged at 1C within a fixed ambient temperature of 25 °C maintained by the thermal chamber. A flowchart diagram for all methods representing the cyclic sequence of charging and discharging is shown in Figure 4. The stop condition during the charging phase (dotted box in Figure 4a) differs for each method, but the discharging phase remains the same for all methods. These charging cycle conditions of each protocol are distinctively shown in Figure 4b, and are also explained below.

- CC method—This charging phase is terminated when the terminal voltage is equal to or above 4.2 V. The T_{ch} and ΔQ_{ch} of this phase are averaged and noted for every 10 cycles (n to $n + 10$ cycles). These T_{ch} and ΔQ_{ch} values are taken as the base values for evaluating the performance of the Li-ion cells for the remaining three methods.
- SCC method—The time length of the sine half-wave from n to $n + 10$ cycles is set equal to T_{ch} and the charging cycle is terminated either when the charging time reaches T_{ch} or the total charge accumulated during the process reaches ΔQ_{ch} , whichever comes first.
- PCC method—The charge cycle termination condition is the same as the SCC method, but this charging protocol has a continuous 10 A pulse train at 0.05 Hz [9] with a 50 percent duty cycle.
- SPCC method—This method also has the same charge cycle termination condition as the SCC method, but in this method, 16 s wide 9.55 A peak sinusoidal half waves with a 4 s relaxation time are generated at the same 0.05 Hz frequency.

The sequence of the current pulses for the PCC and SPCC methods can be observed in the experimental waveforms shown in the following sections.

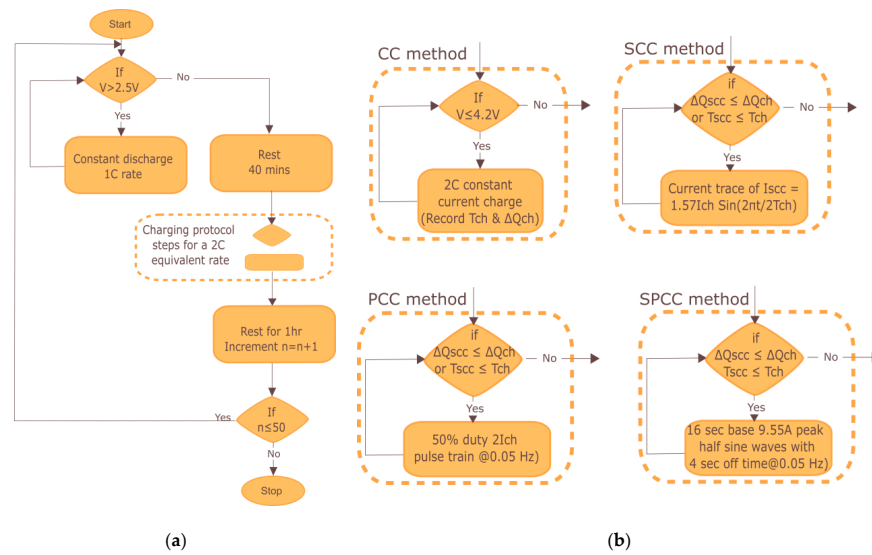


Figure 4. Flowchart of the cyclic testing of the charging protocols. (a) Generalized steps for all four charging methods; (b) charging cycle conditions of each method.

3.1.2. DoD and EIS Testing

Each Li-ion cell under testing is subjected to DoD and EIS at the end of every 50 cycles, and the corresponding detailed flowchart is shown in Figure 5. In this process, first, each Li-ion cell is fully charged at a 0.5 C rate with CC mode followed by CV mode to 4.2 V. After a certain resting time (10 min), it is discharged at a 0.5 C rate with CC mode till 2.5 V, and then followed by CV discharge mode at 2.5 V till 100 mA cut-off is reached. Thus, it ensures the complete discharge of the battery and reaches the exact DoD of the Li-ion cell under testing; hence, the total charge removed is ΔQ_{dch} . Finally, after an additional relaxation time (5 min), the Li-ion cells are again charged at the same rate as CC-CV, but within this process, the intermediate spectrograph tests are performed. These tests are performed when the battery charge is at 0.2, 0.5, and 0.8 times of ΔQ_{dch} and also after the end of the CV mode.

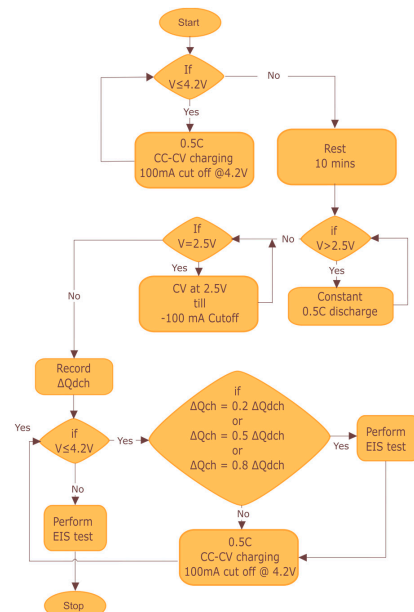


Figure 5. Flowchart for DoD and EIS testing after every 50 cycles of each Li-ion cell.

3.2. Real-Time Experimental Traces

Figure 6 shows the experimental traces of the Li cell's current and change of charge for the flowcharts explained in Section 3.1. Note that the ΔQ_{ch} traces of each method shown in Figure 6a–d are kept the same for all four methods. The relative T_{ch} for PCC and SPCC are observed to be slightly less than (<5%) that of the CC method. In the DoD and EIS testing traces shown in Figure 6e, the discontinuities during the CC phase are the resting time intervals when the EIS tests are performed when the battery charge is 0.2, 0.5, and 0.8 times ΔQ_{dch} .

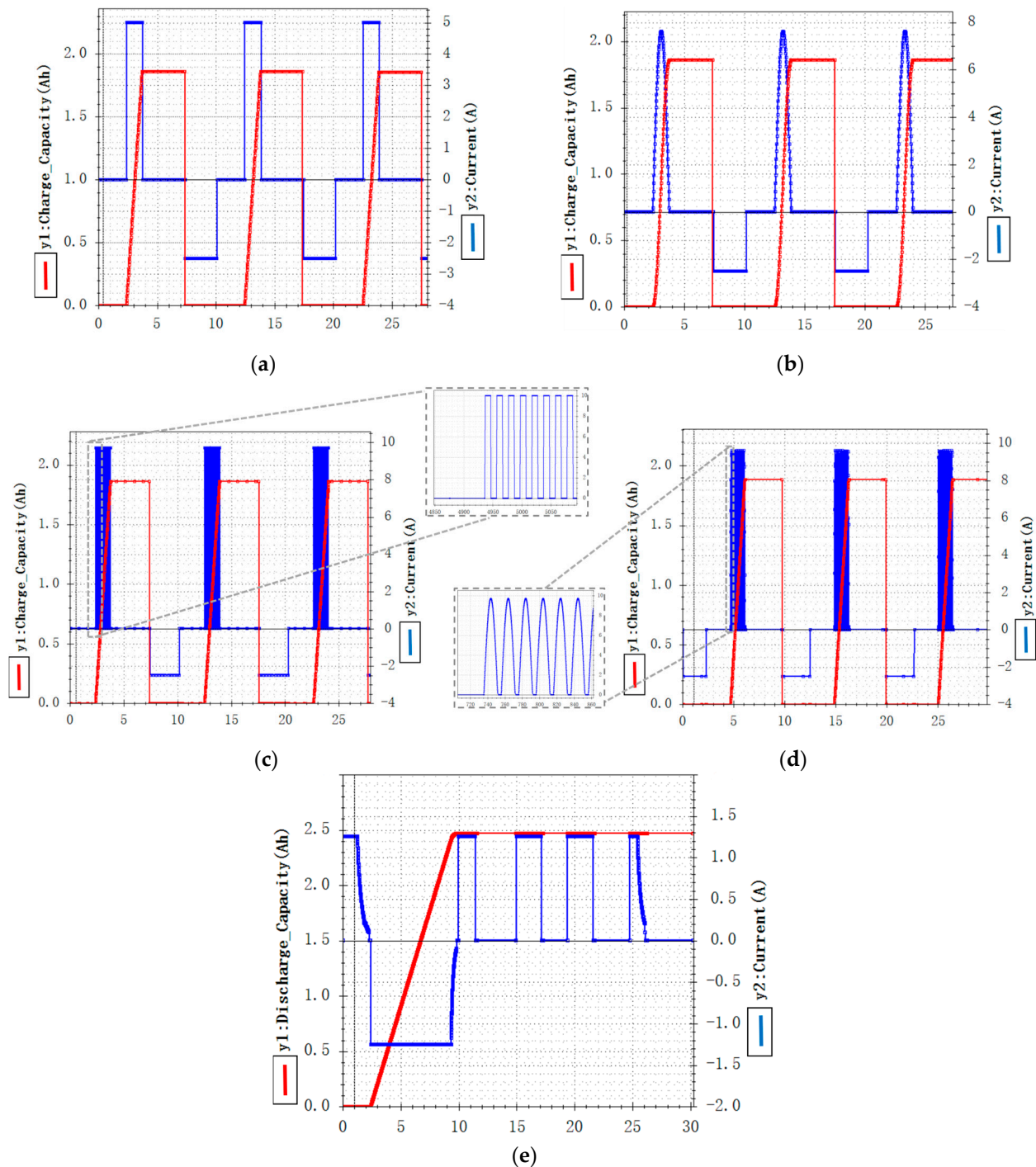


Figure 6. Li-ion cell current (in blue) and Q_{ch} (in red) traces for charge and discharge cycles of (a) CC; (b) SCC; (c) PCC; (d) SPCC protocol; and (e) Li-ion cell current (in blue) and Q_{dch} (in red) traces for DoD and EIS test for every 50 cycles. (Note: x-axis is test time in 10^3 s for all traces.)

Figure 7 shows the experimental traces of the Li cell current and voltages during each charge cycle of the four charging protocols under testing. As discussed in Section 3.1.1, the CC method charge cycle is terminated when the Li cell terminal voltage reaches the maximum voltage of 4.2 V, as can be observed in Figure 8a. However, in the SCC method, most of the charge transfer occurs when the terminal voltage is near the nominal voltage at 3.6 V. Hence, during the SCC method charge cycle, the terminal voltage never hits the Li cell’s maximum voltage rating of 4.2 V, as shown in Figure 8b. However, in the pulsed charging methods (PCC and SPCC), the terminal voltages applied across the Li cell exceed the maximum rating of 4.2 V near the end of the charge cycle. This is carried out to attain the set value of ΔQ_{ch} set by the algorithm, as shown in Figure 6c,d. As the pulsed current peak values of the PCC and SPCC methods are greater than the 5 A constant current of the CC method, the required pulsed voltages are above the maximum 4.2 V to facilitate the same high current flow during the last few pulses of the charging cycle.

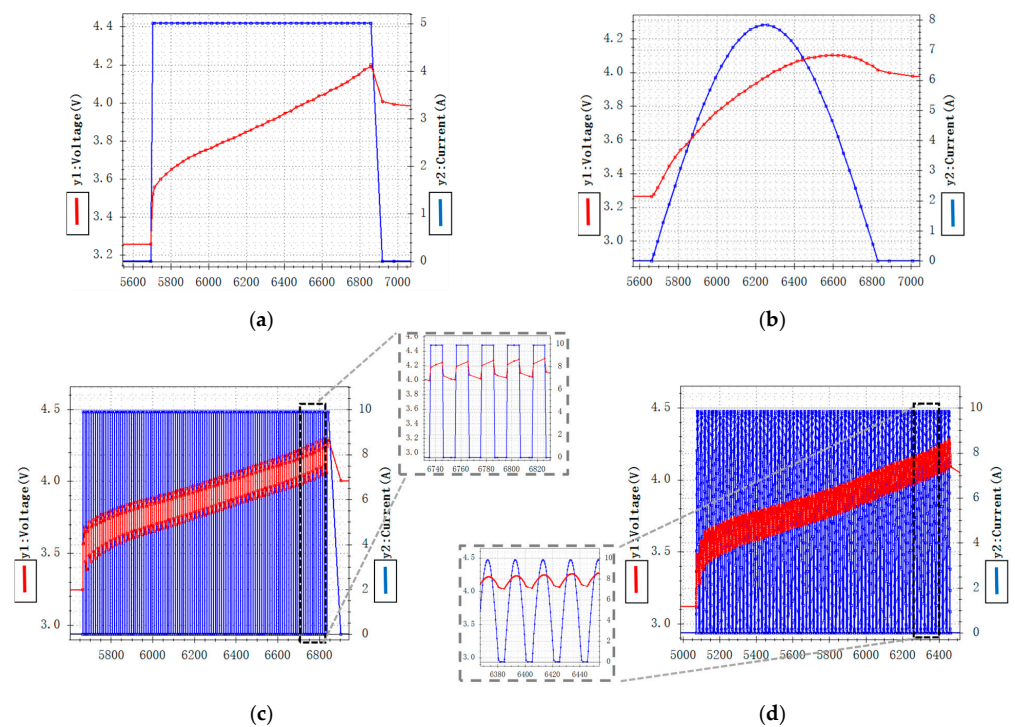


Figure 7. Li-ion cell current (in blue) and voltage (in red) traces for charge cycles of (a) CC; (b) SCC; (c) PCC; and (d) SPCC protocol. (Note: x-axis is test time in seconds for all traces.)

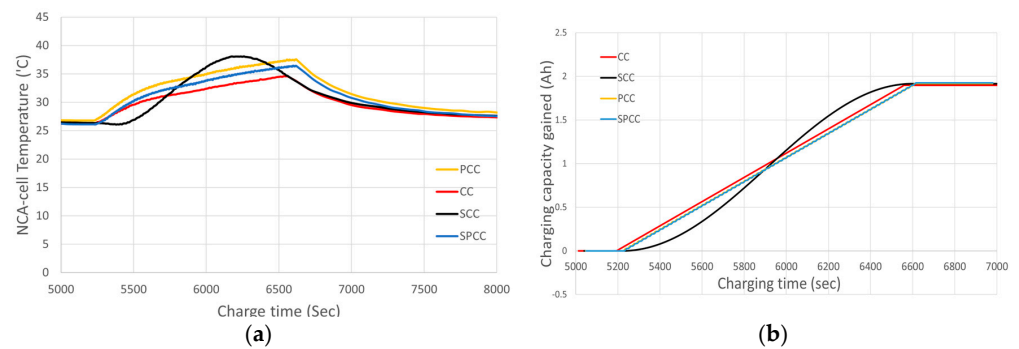


Figure 8. Comparison of (a) surface temperature of Li-ion cell and (b) ΔQ_{ch} trace during the charge cycle of each protocol.

4. Results and Discussion

The surface temperature of the Li-ion cell under each module is plotted and shown in Figure 8a, with the ambient temperature maintained at 25 °C. From Figure 8a, it can be observed that the CC, SCC, PCC, and SPCC methods have peak temperatures of 33.8 °C, 36.8 °C, 37.2 °C, and 35.4 °C, respectively. Hence, the PCC method peaks with the highest temperature change of +12.23 °C because of the 10 A peak pulse currents. The trace of ΔQ_{ch} in the charging phase of each protocol is also plotted and shown in Figure 8b. Observing the ΔQ_{ch} trace, except for SCC, all of the other protocols charge the Li-ion cells at a constant ramp rate. However, only for the SCC method, the rate of charging power is high in the mid-range, i.e., near the nominal voltage, and low near the boundary minimum and maximum voltage levels of the cell.

Figure 9 represents the Nyquist plots of the impedance spectrographs obtained every 50 cycles for each Li-ion cell under testing when implementing the four charging protocols. Note that in each plot, the y-axis corresponds to the negative of the reactive component of the total impedance ($-Z_{imag}$), and the x-axis corresponds to the active component of the total impedance (Z_{real}) (as shown in Figure 1). The radius of the semi-circle in the medium-frequency range corresponds to the charge transfer resistance of the Li cell, and the point of intersection of the curve with the x-axis specifies the effective equivalent ohmic resistance of the cell. These two parameters are helpful in estimating the health of Li cell electrodes.

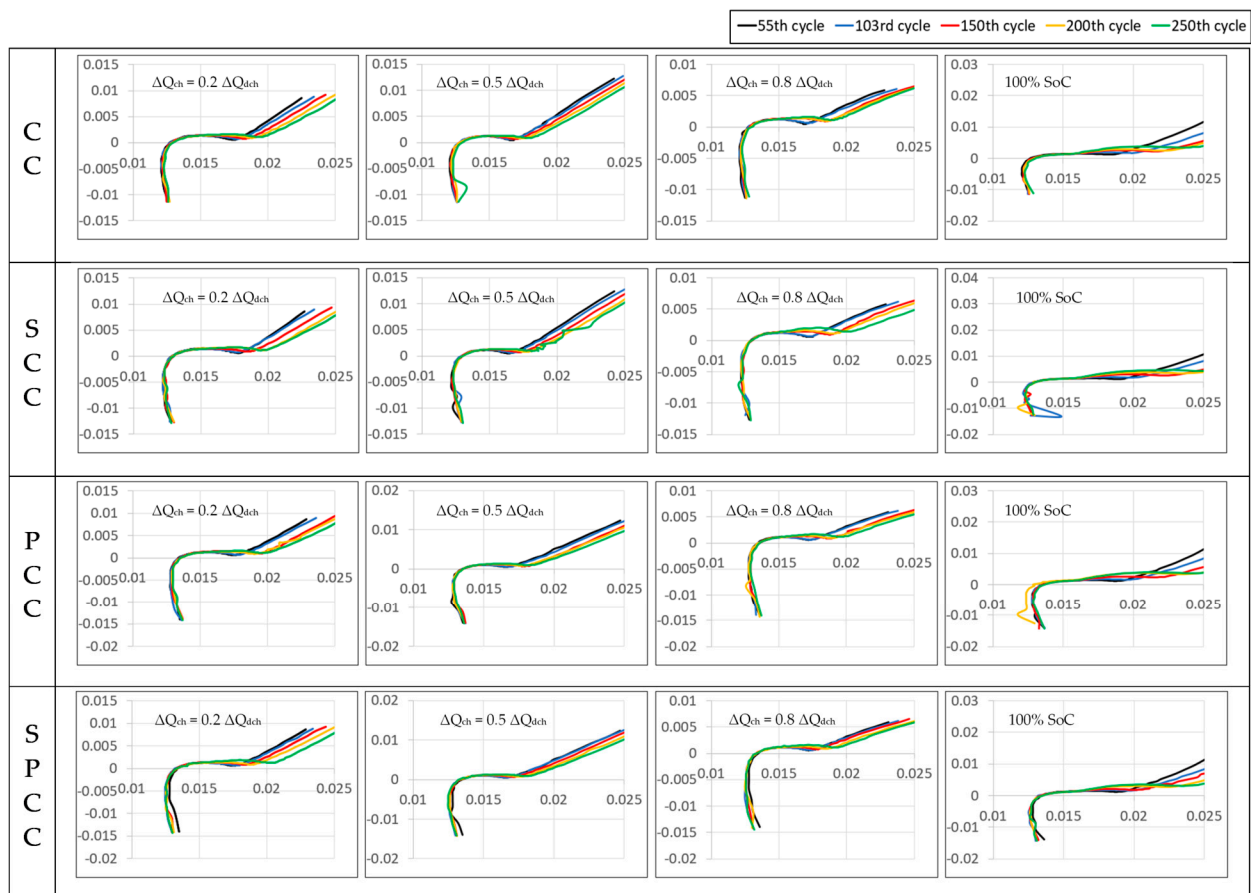


Figure 9. Nyquist plots ($-Z_{imag}$ vs. Z_{real} in ohms) of the impedance spectrographs for NCA cells under testing at charging capacities: $0.2 \times \Delta Q_{dch}$ (subfigures in column 1), $0.5 \times \Delta Q_{dch}$ (subfigures in column 2), $0.8 \times \Delta Q_{dch}$ (subfigures in column 3), and 100% SoC (subfigures in column 4), obtained every 50 cycles till the 250th life cycle.

Figure 10 presents the plots related to the performance evaluation of the Li cells tested under the four fast charging protocols. Among the four columns of Figure 9, the third column with the Nyquist curves of $0.8 \times \Delta Q_{dch}$ has noticeable differences in the medium-frequency range compared to the other columns. For a clear comparison, the Nyquist curves only corresponding to the medium-frequency range at the 250th cycle of the Li cells corresponding to each charging method (CC, SCC, PCC, and SPCC) are redrawn in Figure 10a. From Figure 10a, it can be observed that the SCC method has the highest and the SPCC method has the lowest increase in the size of the medium-frequency semi-circle. Therefore, the SPCC method has the lowest and SCC has the highest charge transfer effect among the four charging methods. This implies that the rate of electrode surface degradation is greater with the SCC method and lower with the SPCC method [6,13]. Considering the ohmic effect shown in Figure 10a, the point of intersection B (between the Nyquist curve and the x-axis) for the pulsed charging methods (PCC and SPCC) is slightly further away from the origin when compared with the point of intersection A from the non-pulsed charging methods (CC and SCC). Hence, it is noted that the pulsed-current method increases the equivalent ohmic resistance of the Li cells. Collectively, the PCC method impacted both the charge transfer and ohmic resistance of the NMC-chemistry-based Li cell.

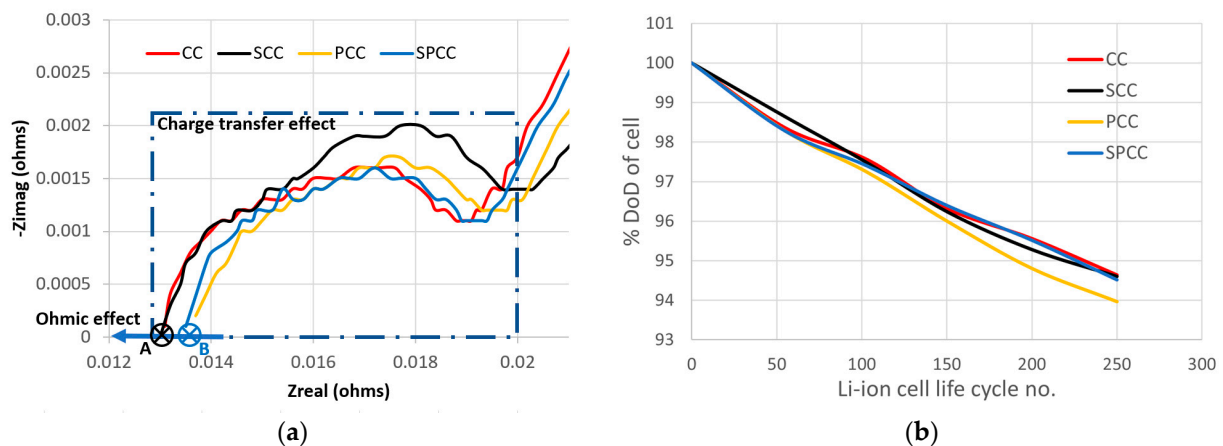


Figure 10. Performance evaluation of Li cells under testing. (a) Nyquist plots for $0.8 \times \Delta Q_{dch}$ after 250 cycles of the Li cells for the four charging methods; (b) plot of the capacity degradation in Li cells corresponding to the four fast charging protocols tested for 250 cycles (DoD test performed every 50 cycles).

Using the ΔQ_{dch} values obtained from the DoD tests performed every 50 life cycles, a plot of the capacity degradation was created for the Li cells, as shown in Figure 10b. At the end of 250 cycles, as can be observed from Figure 10, the health of the Li cell under the PCC method showed the highest degradation compared with the other protocols. According to the results presented in [9], the 0.05 Hz low-frequency PCC protocol extended the battery lifetime by more than 50% when tested on NMC chemistry Li-cells. In contrast, the same 0.05 Hz PCC test on NCA cells showed a negative impact on the battery life. However, it has to be noted that the proposed SCC and SPCC methods do not show much deviation in terms of capacity degradation compared with the regular CC method.

5. Conclusions

In this paper, SCC and SPCC charging methods were investigated on NCA-based Li-ion cells, and their performance was evaluated in comparison with the conventional CC and PCC charging methods. According to the EIS evaluation, the SPCC method showed the lowest rate of increase in charge transfer resistance compared with the other methods. After testing for 250 cycles during the experiment, it was observed that the low-frequency 0.05 Hz PCC method degraded the NCA cell capacity faster than the CC method. However, the SCC and SPCC methods showed almost the same capacity degradation as the CC

method. Although these methods may hold the same life cycle time as the CC method, the SCC and SPCC methods have their own benefits other than life cycle extension.

In future, when ultra-fast chargers will have the major power share in the grid, the implementation of the SCC charging method with slow and gradual power loading will help to avoid sudden loading transients, thereby causing less disturbance to the dynamic performance of the grid. In smart grids with demand-side communication, this predefined SCC loading will help to forecast the charging load demand every 10 min. On the other hand, bringing the SPCC method frequencies closer to grid frequency can help to eliminate the DC-DC stage in the charger, which can considerably improve the power density and efficiency of the EV charger. Thus, they provide an economically viable solution for an EV charger being deployed with minimal change in the infrastructure.

Author Contributions: Conceptualization, S.B.A. and K.R.; methodology, S.B.A.; validation, S.B.A. and T.D.; formal analysis, S.B.A.; investigation, S.B.A. and T.D.; resources, K.R.; supervision, K.R.; writing—original draft, S.B.A. and T.D. All authors have read and agreed to the published version of the manuscript.

Funding: The authors gratefully acknowledge the partial financial support of the Sandia National Labs, which is funded by the Office of Electricity at U.S. DOE.

Data Availability Statement: Data is contained within the article.

Acknowledgments: The authors would like to thank the scientists of Sandia National Labs for their support.

Conflicts of Interest: The authors declare no conflicts of interest.

References

1. Safayatullah, M.; Elrais, M.T.; Ghosh, S.; Rezaei, R.; Batarseh, I. A Comprehensive Review of Power Converter Topologies and Control Methods for Electric Vehicle Fast Charging Applications. *IEEE Access* **2022**, *10*, 40753–40793. [[CrossRef](#)]
2. Dubarry, M.; Truchot, C.; Cugnet, M.; Liaw, B.Y.; Gering, K.; Sazhin, S.; Jamison, D.; Michelbacher, C. Evaluation of commercial lithium-ion cells based on composite positive electrode for plug-in hybrid electric vehicle applications. Part I: Initial characterizations. *J. Power Sources* **2011**, *196*, 10328–10335. [[CrossRef](#)]
3. Goel, S.; Sharma, R.; Rathore, A.K. A review on barrier and challenges of electric vehicle in India and vehicle to grid optimization. *J. Transp. Eng.* **2021**, *4*, 100057. [[CrossRef](#)]
4. Huang, X.; Li, Y.; Acharya, A.B.; Sui, X.; Meng, J.; Teodorescu, R.; Stroe, D.I. A review of pulsed current technique for lithium-ion batteries. *Energies* **2020**, *13*, 2458. [[CrossRef](#)]
5. Keil, P.; Jossen, A. Charging protocols for lithium-ion batteries and their impact on cycle life—An experimental study with different 18650 high-power cells. *J. Energy Storage* **2016**, *6*, 125–141. [[CrossRef](#)]
6. Abdel-Monem, M.; Trad, K.; Omar, N.; Hegazy, O.; Van den Bossche, P.; Van Mierlo, J. Influence analysis of static and dynamic fast-charging current profiles on ageing performance of commercial lithium-ion batteries. *J. Energy* **2017**, *120*, 179–191. [[CrossRef](#)]
7. Fang, H.; Depcik, C.; Lvovich, V. Optimal pulse-modulated Lithium-ion battery charging algorithms. *J. Energy Storage* **2018**, *15*, 359–367. [[CrossRef](#)]
8. Huang, X.; Jin, S.; Meng, J.; Teodorescu, R.; Stroe, D.-I. The Effect of Pulsed Current on the Lifetime of Lithium-ion Batteries. In Proceedings of the 2021 IEEE Energy Conversion Congress and Exposition (ECCE), Vancouver, BC, Canada, 10–14 October 2021; pp. 1724–1729.
9. Huang, X.; Liu, W.; Meng, J.; Li, Y.; Jin, S.; Teodorescu, R.; Stroe, D.-I. Lifetime Extension of Lithium-Ion Batteries with Low-Frequency Pulsed Current Charging. *IEEE J. Emerg. Sel. Top. Power Electron.* **2023**, *11*, 57–66. [[CrossRef](#)]
10. Huang, X.; Meng, J.; Liu, W.; Ru, F.; Duan, C.; Xu, X.; Stroe, D.-I.; Teodorescu, R. Lithium-Ion Battery Lifetime Extension with Positive Pulsed Current Charging. *IEEE Trans. Ind. Electron.* **2024**, *71*, 484–492. [[CrossRef](#)]
11. Li, J.; Murphy, E.; Winnick, J.; Kohl, P.A. The effects of pulse charging on cycling characteristics of commercial Lithium-ion batteries. *J. Power Sources* **2001**, *102*, 302–309. [[CrossRef](#)]
12. Kannan, D.R.; Weatherspoon, M.H. The Effect of Pulse Charging on Commercial Lithium Cobalt Oxide (LCO) Battery Characteristics. *J. Electrochem. Sci.* **2021**, *16*, 210453. [[CrossRef](#)]
13. Lv, H.; Huang, X.; Liu, Y. Analysis on pulse charging–discharging strategies for improving capacity retention rates of lithium-ion batteries. *Ionics* **2020**, *26*, 1749–1770. [[CrossRef](#)]
14. Monem, M.A.; Trad, K.; Omar, N.; Hegazy, O.; Mantels, B.; Mulder, G.; Van den Bossche, P.; Van Mierlo, J. Lithium-ion batteries: Evaluation study of different charging methodologies based on aging process. *Appl. Energy* **2015**, *152*, 143–155. [[CrossRef](#)]
15. Huang, X.; Liu, W.; Acharya, A.B.; Meng, J.; Teodorescu, R.; Stroe, D.-I. Effect of Pulsed Current on Charging Performance of Lithium-Ion Batteries. *IEEE Trans. Ind. Electron.* **2022**, *69*, 10144–10153. [[CrossRef](#)]

16. Cho, S.-Y.; Lee, I.-O.; Baek, J.-I.; Moon, G.-W. Battery Impedance Analysis Considering DC Component in Sinusoidal Ripple-Current Charging. *IEEE Trans. Ind. Electron.* **2016**, *63*, 1561–1573. [[CrossRef](#)]
17. Chen, L.R.; Wu, S.L.; Shieh, D.T.; Chen, T.R. Sinusoidal-ripple-current charging strategy and optimal charging frequency study for Li-ion batteries. *IEEE Trans. Ind. Electron.* **2012**, *60*, 88–97. [[CrossRef](#)]
18. Jiang, B.; Berliner, M.D.; Lai, K.; Asinger, P.A.; Zhao, H.; Herring, P.K.; Bazant, M.Z.; Braatz, R.D. Fast charging design for Lithium-ion batteries via Bayesian optimization. *Appl. Energy* **2022**, *307*, 118244. [[CrossRef](#)]
19. Guo, Z.; Liaw, B.Y.; Qiu, X.; Gao, L.; Zhang, C. Optimal charging method for lithium-ion batteries using a universal voltage protocol accommodating aging. *J. Power Sources* **2015**, *274*, 957–964. [[CrossRef](#)]

Disclaimer/Publisher's Note: The statements, opinions and data contained in all publications are solely those of the individual author(s) and contributor(s) and not of MDPI and/or the editor(s). MDPI and/or the editor(s) disclaim responsibility for any injury to people or property resulting from any ideas, methods, instructions or products referred to in the content.